J. Pestic. Sci. **46**(1), 75–87 (2021)
DOI: 10.1584/jpestics.D20-072

JOURNAL OF PESTICIDE SCIENCE

Regular Article

Non-steroidal inhibitors of *Drosophila melanogaster* steroidogenic glutathione *S*-transferase Noppera-bo

Kotaro Koiwai,[1,†] Kana Morohashi,[2,†] Kazue Inaba,[1,2] Kana Ebihara,[2] Hirotatsu Kojima,[3] Takayoshi Okabe,[3] Ryunosuke Yoshino,[4] Takatsugu Hirokawa,[5,6,7] Taiki Nampo,[8] Yuuta Fujikawa,[8] Hideshi Inoue,[8] Fumiaki Yumoto,[1] Toshiya Senda[1,9,10] and Ryusuke Niwa[1,2,11,*]

[1] *Structural Biology Research Center, Photon Factory, Institute of Materials Structure Science, High Energy Accelerator Research Organization, 1–1 Oho, Tsukuba, Ibaraki 305–0801, Japan*
[2] *Graduate School of Life and Environmental Sciences, University of Tsukuba, 1–1–1 Tennodai, Tsukuba, Ibaraki 305–8572, Japan*
[3] *Drug Discovery Initiative, The University of Tokyo, 7–3–1 Hongo, Bunkyo-ku, Tokyo 113–0033, Japan*
[4] *Graduate School of Comprehensive Human Sciences Majors of Medical Sciences, University of Tsukuba, 1–1–1 Tennodai, Tsukuba, Ibaraki 305–8575, Japan*
[5] *Transborder Medical Research Center, University of Tsukuba, 1–1–1 Tennodai, Tsukuba, Ibaraki 305–8575, Japan*
[6] *Division of Biomedical Science, Faculty of Medicine, University of Tsukuba, 1–1–1 Tennodai, Tsukuba, Ibaraki 305–8575, Japan*
[7] *Molecular Profiling Research Center for Drug Discovery, National Institute of Advanced Industrial Science and Technology, 2–4–7 Aomi, Koto-ku, Tokyo 135–0064, Japan*
[8] *School of Life Sciences, Tokyo University of Pharmacy and Life Sciences, 1432–1 Horinouchi, Hachioji, Tokyo 192–0392, Japan*
[9] *School of High Energy Accelerator Science, SOKENDAI University, 1–1 Oho, Tsukuba, Ibaraki 305–0801, Japan*
[10] *Faculty of Pure and Applied Sciences, University of Tsukuba, 1–1–1 Tennodai, Ibaraki 305–8571, Japan*
[11] *Life Science Center for Survival Dynamics, Tsukuba Advanced Research Alliance (TARA), University of Tsukuba, 1–1–1 Tennodai, Tsukuba, Ibaraki 305–8577, Japan*

(Received October 31, 2020; Accepted January 7, 2021)

Supplementary material

Insect growth regulators (IGRs) can be developed by elucidating the molecular mechanisms of insect-specific biological events. Because insect molting, and metamorphosis are controlled by ecdysteroids, their biosynthetic pathways can serve as targets for IGR development. The glutathione *S*-transferase Noppera-bo (Nobo), which is conserved in dipteran and lepidopteran species, plays an essential role in ecdysteroid biosynthesis. Our previous study using 17β-estradiol as a molecular probe revealed that Asp113 of *Drosophila melanogaster* Nobo (DmNobo) is essential for its biological function. However, to develop IGRs with a greater Nobo inhibitory activity than 17β-estradiol, further structural information is warranted. Here, we report five novel non-steroidal DmNobo inhibitors. Analysis of crystal structures of complexes revealed that DmNobo binds these inhibitors in an Asp113-independent manner. Among amino acid residues at the substrate-recognition site, conformation of conserved Phe39 was dynamically altered upon inhibitor binding. Therefore, these inhibitors can serve as seed compounds for IGR development.

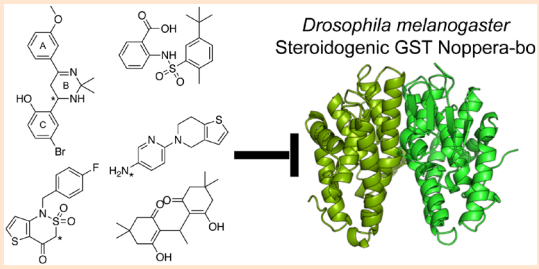

Keywords: insect growth regulator, ecdysone, ecdysteroid, glutathione *S*-transferase, structure–activity relationship.

* To whom correspondence should be addressed.
E-mail: ryusuke-niwa@tara.tsukuba.ac.jp
† These authors contributed equally to this work.
Published online February 4, 2021

Introduction

Insect growth regulators (IGRs) are chemical compounds that specifically inhibit the growth of insects without producing adverse effects on other animals.[1)] To identify and develop IGRs, insect-specific molecular, cellular, and systemic regulatory mechanisms of insect growth must be elucidated. One of

the IGR targets that has historically received great attention is ecdysteroid, which plays pivotal roles in regulating the development and physiology of arthropods, including insects.[2] Since ecdysteroids are not present in animals other than arthropods, molecules involved in their biosynthesis, secretion, circulation, and reception may serve as potent targets for IGR development.

Ecdysteroids are biosynthesized from dietary sterols.[2,3] Each reaction in the biosynthetic pathway of the ecdysteroid 20-hydroxyecdysone (20E) is catalyzed by a specific ecdysteroidogenic enzyme.[3,4] Several of these enzymes have been identified over the last two decades, including Noppera-bo (Nobo),[5–7] Neverland,[8,9] Non-molting glossy/Shroud,[10] Spook/CYP307A1,[11,12] Spookier/CYP307A2,[12] CYP6T3,[13] Phantom/CYP306A1,[14,15] Disembodied/CYP302A1,[16] Shadow/CYP315A1,[16] and Shade/CYP314A1.[17] Loss-of-function mutations of genes encoding these enzymes result in developmental lethality. Specifically, in *Drosophila melanogaster*, complete loss-of-function mutants of *nobo*, *shroud*, *spook*, *phantom*, *disembodied*, *shade*, and *shadow*, often classified as Halloween mutants, typically exhibit embryonic lethality due to loss of differentiated cuticular structures.[18] Thus far, the functions of these enzymes have been characterized genetically and some of them have also been analyzed biochemically.[3,19]

Among the Halloween genes, *nobo* encodes a member of the epsilon class of cytosolic glutathione *S*-transferases (GSTs, EC 2.5.1.18; hereafter GSTEs).[20–22] Typically, glutathione (GSH) binds to the GSH-binding site (G-site) of GST, while other substrates bind to its hydrophobic site (H-site). GST mainly catalyzes the following three reactions with GSH: GSH conjugation to a substrate, reduction of the substrate, and isomerization of the formed complex.[23] Previous studies have demonstrated that *nobo* is specifically expressed in the prothoracic gland and adult ovary, both of which biosynthesize ecdysteroids.[5–7] In *D. melanogaster* and *Bombyx mori*, loss-of-function mutations of *nobo* result in developmental lethality, which can be rescued by 20E administration.[5–7] In addition, *D. melanogaster* mutants can be rescued by cholesterol, which is the most upstream compound of the ecdysteroid biosynthetic pathway.[6] Consistent with the requirement of GSH for GST function, defects in GSH biosynthesis in *D. melanogaster* lead to larval lethality, which can be partially rescued by 20E or cholesterol administration.[24] Together, these reports indicate that although an endogenous ligand of Nobo other than GSH has not been elucidated, the *nobo* family genes are essential for ecdysteroid biosynthesis through regulating cholesterol trafficking and/or metabolism. As *nobo* is conserved only in dipteran and lepidopteran species,[20–22] Nobo can serve as a potent target for developing IGRs that disrupt the life cycle of only specific insects.

We have previously reported that the vertebrate female sex hormone 17β-estradiol (EST) inhibited *in vitro* GSH conjugation activity of *D. melanogaster* Nobo (DmNobo).[25] Our integrated analysis revealed that Asp113 is essential for EST binding to the H-site of GST and *in vivo* functions of Nobo.[22] However, inhibitory effects of compounds other than EST should be identified for IGR development, because EST may act as an endocrine disruptor in vertebrates. Therefore, non-steroidal DmNobo inhibitors identified from a chemical compound library must be analyzed. Here, we report five novel inhibitors and some derivatives of DmNobo as well as the crystal structures of their complexes with DmNobo. These inhibitors do not interact with Asp113 and induce a conformational change of Phe39. Our findings offer a novel strategy for IGR development.

Materials and methods

1. Chemical compounds

A chemical library containing 9,600 compounds was provided by the Drug Discovery Initiative (DDI), The University of Tokyo, Japan. TDP011 (IUPAC name: 4-bromo-2-[4-(3-methoxyphenyl)-2,2-dimethyl-5,6-dihydro-1*H*-pyrimidin-6-yl]phenol) and TDP012 (IUPAC name: 1-(4-fluorobenzyl)-1*H*-thieno[3,2-c][1,2]thiazin-4(3*H*)-one 2,2-dioxide) were purchased from ChemDiv (Cat# K915-0968 and C200-3720, respectively). TDP044 (IUPAC name: 2,2′-(1,1-ethanediyl)bis(3-hydroxy-5,5-dimethyl-2-cyclohexen-1-one) was purchased from Labotest (Cat# LT00014582). TDP045 (IUPAC name: 5,5-dimethyl-1,3-cyclohexanedione) was purchased from Fluorochem (Cat# 011151). 3,4-DNADCF was prepared as previously described.[25] TDP013 (IUPAC name: 2-(5-*tert*-butyl-2-methyl-benzenesulfonylamino)-benzoic acid, PubChem CID: 2360625), TDP015 (IUPAC name: 6-(6,7-dihydrothieno[3,2-c]pyridin-5(4*H*)-yl)-3-pyridinamine, PubChem CID: 1677781) and TDP046 were synthesized as described in Supplementary Information (Schemes S1–S3, Supplementary Methods).

2. Protein expression, purification, and crystallization

The DmNobo protein was expressed, purified, and crystallized as previously described.[22] Briefly, DmNobo was expressed in *Escherichia coli* BL21 (DE3) harboring the pCold III_DmNobo plasmid and purified by GSH affinity chromatography with Glutathione Sepharose 4B (Cytiva, Tokyo, Japan) and size-exclusion chromatography with Superdex 200 HiLoad 16/600 (Cytiva). Conditions of the reservoir solution for DmNobo crystallization were optimized as 34% (v/v) PPG400 in 80 mM Bis-Tris (pH 6.4). Crystals of substrate complexes were prepared by soaking them in artificial mother liquor (42.5% [v/v] PPG 400 in 100 mM Bis-Tris [pH 6.4]) containing each of 30 mM compound with or without 10 mM GSH for 2 days.

3. GST activity inhibition assay

High-throughput screening for DmNobo inhibitors using a 384-well format (20 μL per well) with 9,600 small molecules from a chemical library (DDI, The University of Tokyo) was conducted as previously described.[25] Then, *in vitro* GST activity inhibition assay was performed to determine the 50% inhibitory concentration (IC_{50}) values of six chemical compounds (Fig. 2), as described by Koiwai *et al.*,[22] with minor modifications. Compound solutions were prepared as follows: TDP011, TDP012,

TDP013, and TDP015 were dissolved to 2.5 mM and TDP045 to 100 mM in DMSO. Dilution series of compounds, ranging from 100 mM to 5.1 μM for TDP016 and from 2.5 mM to 4.9 μM for all other compounds were prepared by two-fold serial dilution with their solvents. Next, 5 μL of each compound solution in the dilution series was mixed with 245 μL of solution A (100 mM sodium phosphate buffer [pH 6.5], 0.01% Tween 20, 2 mM GSH, 50 ng·mL^{-1} DmNobo protein), and 100 μL of the mixture was dispensed on a 96-well plate. Then, 100 μL of solution B (2 μM 3,4-DNADCF and 100 mM sodium phosphate buffer [pH 6.5]) was added to each well. In summary, the final reaction system was composed of 100 mM sodium phosphate buffer [pH 6.5], 25 ng·mL^{-1} DmNobo protein, 1 mM GSH, 0.005% Tween 20, and 1 μM 3,4-DNACDF. The GSH-conjugated product was excited at 485 nm, and the fluorescence intensity at 538 nm was measured every 30 sec for 3 min using Fluoroskan Ascent FL (Thermo Fisher Scientific, Waltham, USA). The IC_{50} values were calculated as described by Koiwai *et al.*[22] The assay was performed in duplicate.

4. Crystal structure determination

Crystals of proper size were picked up with MicroLoop (MiTeGen, New York, USA), flash-frozen in liquid nitrogen, and stored in Uni-Pucks (Molecular Dimensions, Ohio, USA). Diffraction data were collected at beamlines BL-1A, BL-5A, BL-17A, and AR NE-3A of the Photon Factory in KEK (Tsukuba, Japan) and at beamline 5A of the Taiwan Photon Source (Hsinchu, Taiwan). The diffraction datasets collected from the Photon Factory were automatically processed and scaled using XDS,[26] POINTLESS,[27] and AIMLESS,[28] which are integrated in PReMo,[29] and those collected from the Taiwan Photon Source were processed and scaled using XDS and AIMLESS. Crystallographic statistics are summarized in supplemental Table S1.

For automated protein crystallography, we developed the software PEINTS (https://github.com/KotaroKoiwai/PEINTS), in which phases of crystal structures can be determined by the molecular replacement (MR) method with MOLREP[30] using the crystal structure of the apo form of DmNobo (PDB ID=6KEN) as a search model. Molecular models were initially refined using REFMAC5.[31] Models were built manually using COOT,[32] and the molecular models were further refined with PHENIX.REFINE.[33] Simulated annealing m*F*o–D*F*c omit-maps of compounds and GSH were calculated using PHENIX.REFINE. Interactions between DmNobo and GSH or compounds were analyzed using PoseView[34] and Discovery Studio Visualizer (Dassault Systèmes BIOVIA, Discovery Studio Modeling Environment, Release 2020, San Diego: Dassault Systèmes, 2019). The volume of DmNobo binding cavity was calculated using the Channel Finder program in 3V,[35] with radii of 4 and 1 Å for the outer and inner probes, respectively. The root-mean-square deviation (RMSD) values from the least-squares fitting of the DmNobo structures were calculated using GESAMT.[36] Atom pairs within a 4.0 Å distance were defined as direct contacts. All molecular graphics were prepared using the PyMOL Molecular Graphics System version 1.7.6 (Schrödinger, NY, USA).

The X-ray data and coordinates presented in this study are deposited in the Protein Data Bank (PDB; https://pdbj.org/) under the PDB IDs 7DAX, 7DAY, 7DAZ, 7DB0, 7DB1, 7DB2, 7DB3, and 7DB4.

5. Molecular dynamics simulations

Molecular dynamics (MD) simulations for DmNobo–Apo (PDB ID: 6KEO) and DmNobo–GSH (PDB ID: 6KEN) were performed as previously described.[22] The structures were processed to assign bond orders and hydrogenation. The ionization states of GSH at pH 7.0±2.0 were predicted using Epik,[37] and H-bond optimization was conducted using PROPKA.[38] Energy minimization was performed in Maestro using the OPLS3 force field.[39] Preparation for MD simulations was conducted using the Molecular Dynamics System Setup Module of Maestro (Schrödinger, NY, USA). DmNobo-Apo and DmNobo-GSH were subjected to energy minimization and placed in an orthorhombic box with a buffer distance of 10 Å to create a hydration model, and the TIP3P water model[40] was used for the hydration model. NaCl (0.15 M) served as the counterion to neutralize the system. The MD simulations were performed using Desmond software, version 2.3 (Schrödinger, NY, USA). The cut-off radii for van der Waals was 9 Å. The cut-off values of the time step, initial temperature, and pressure of the system were set to 2.0 fs, 300 K, and 1.01325 bar, respectively. The sampling interval during the simulation was set to 10 ps. Finally, we performed MD simulations using the NPT ensemble for 100 nsec.

Results

1. Identification of DmNobo inhibitors by high-throughput screening

We performed high-throughput screening for the inhibitors of GSH conjugation activity of DmNobo using the artificial fluorescent substrate 3,4-DNADCF. From 9,600 chemical compounds obtained from DDI,[25] we identified six compounds with IC_{50} values below 10 μM. One of the inhibitors was EST, which has a steroidal backbone similar to ecdysteroids.[22,25] The other five compounds did not have a steroidal backbone and were designated TDP011 (IC_{50}=6.72±1.48 μM), TDP012 (IC_{50}=3.10±0.77 μM), TDP013 (IC_{50}=8.94±1.65 μM), TDP015 (IC_{50}=3.32±0.81 μM), and TDP044 (IC_{50}=0.62±0.52 μM) compared with EST (IC_{50}=2.33±0.08 μM) (Figs. 1, 2, Table 1). Since these compounds have various chemical structures, we expected them to bind with DmNobo in a different manner from EST.

2. Crystal structures of DmNobo complexed with the five inhibitors and their derivatives

To examine the structure–activity relationships of the novel inhibitors identified, we determined the crystal structures of their complexes with DmNobo (Supplemental Table S1). The resolutions of these structures were in the range of 1.40 to 1.80 Å, and inhibitor and water molecules could be clearly identified (Supplemental Fig. S1).

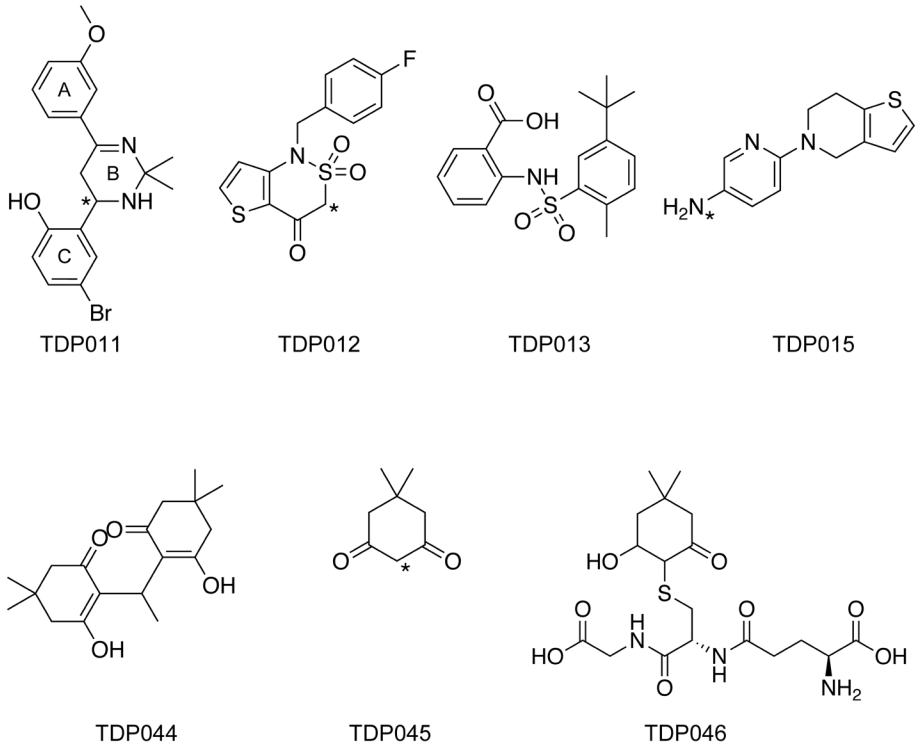

Fig. 1. Chemical structures of the newly identified DmNobo inhibitors and their derivatives. TDP011, TDP012, TDP013, TDP015, and TDP044 were identified as hit compounds in high-throughput screening. The 6-membered rings of TDP011 are labeled with A, B, and C. Asterisk indicates the GS-adduct site in crystal structure.

TDP044 possesses two dimedone ring structures (Fig. 1). Of note, a DmNobo crystal soaked in a solution containing TDP044 showed clear electron densities corresponding to only one dimedone-ring in either chain A or B (Supplemental Fig. S1 F). Although we have collected data from crystals soaked under various conditions, a clear electron density map for TDP044 was not observed. The reason behind such a change in the crystal remains unclear, possibly because of degradation or oxidation of TDP044 during soaking. Based on this observation, we examined whether dimedone (hereafter TDP045) physically interacted with DmNobo and inhibited its enzymatic activity. We determined the crystal structure of DmNobo complexed with TDP045. Although TDP045 did not exhibit a strong inhibitory activity against DmNobo (Fig. 2), the electron density of TDP045 could be clearly observed (Supplemental Fig. S1 G and H). Therefore, although TDP045 cannot be classified as a DmNobo inhibitor *per se*, we decided to include TDP045 instead of TDP044 for further crystal structure analysis to understand the possible mode of action of TDP044, a TDP045 derivative.

Although all compounds showed binding at the H-site, they could be categorized into two classes based on the GSH-dependency of their interaction with DmNobo. Crystallographic analysis with and without GSH revealed that the interactions of TDP011, TDP012, and TDP015 with DmNobo were GSH-dependent, while those of TDP013 and TDP045 with DmNobo were GSH-independent (Table 1).

For comprehensive comparison, the DmNobo–inhibitor complex structures determined in this study and those reported in previous studies were mutually superposed by least-squares fitting using Cα atoms (Supplemental Table S2). The RMSD values were 0.14–0.48 Å for superpositions of the Cα atoms of chain A and 0.15–0.97 Å for superpositions of the Cα atoms of chains A and B (Supplemental Table S2), indicating that it is reasonable to consider that these crystal structures were essentially the same as one another, and no large-scale conformational changes occurred upon compound and/or GSH binding. Structural comparison, however, revealed several local conformational changes induced by compound binding (see below).

3. Residues interacting with the identified compounds

Interactions between compounds and residues at the H-site were analyzed using PoseView and Discovery Studio (Fig. 3). The analysis revealed that Pro15, Leu38, Phe39, Phe110, Met117, Val121, Leu208, Thr211, Met212, and Val215 were involved in hydrophobic interactions with compounds, while Ser14 and Ser114 formed specific hydrophilic interactions. Leu38 and Met117 interacted with the compounds most frequently. All inhibitors, except TDP045, interacted with three to seven hydrophobic residues at the H-site. Among hydrophobic residues at the H-site, Phe39 largely contributes to hydrophobic interactions with EST.[22] However, TDP012 and TDP013 in a GSH-free form did not interact with the side chain of Phe39, suggesting that this side chain is not always necessary for hydrophobic interactions with the compounds.

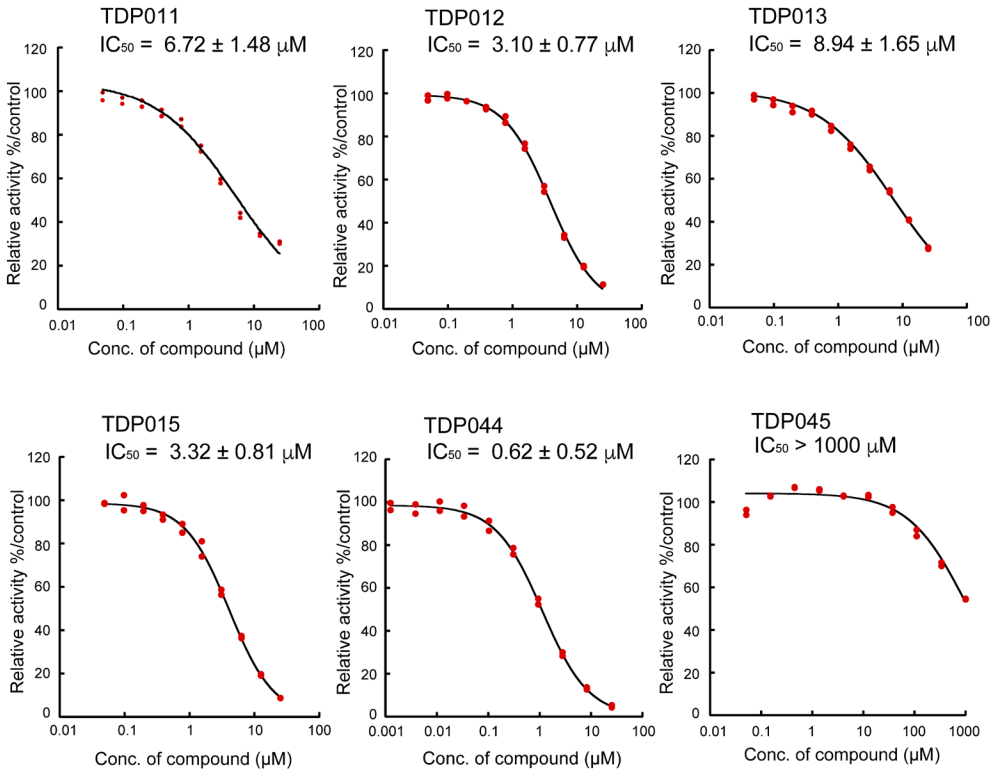

Fig. 2. Compound-dependent inhibition of the GSH-conjugation activity of DmNobo. 3,4-DNADCF was used as an artificial fluorescent substrate. Relative activity is defined as the ratio of activity with and without the compounds. All data points in the assay are indicated. The error values of IC_{50} were calculated with standard deviation from duplicate assays.

4. GSH-independent interactions

TDP013 and TDP045 could bind DmNobo without GSH. Of note, the conformation of these two compounds at the H-site was altered upon GSH binding through interaction or conjugation with GSH (Fig. 4A and 4B).

In the absence of GSH, TDP013 conformation was such that the planes of the two rings were roughly parallel to the α-helices. A large cavity, the G-site, was placed above the bound TDP013, and the unoccupied G-site was filled with water molecules, forming a hydrogen bond network. In the presence of GSH, TDP013 rotated at the H-site, assuming a conformation in which the planes of the rings were roughly perpendicular to the α-helices. This change likely resulted from the clash between the thiol group of GSH and TDP013. The rearrangement of TDP013 induced another conformational change of Phe39 (see below).

In the absence of GSH, TDP045 was located deep inside the H-site. One of the carbonyl groups of TDP045 interacted with Asp113 (2.6 Å), and the other formed a hydrogen bond with Ser114 (2.7 Å). While the IC_{50} value of TDP045 was substantially larger than those of other compounds, its electron density could be clearly observed, suggesting that the binding of TDP045 is stable, at least in the crystal. Upon GSH binding, TDP045 ro-

Table 1. Characters of DmNobo inhibitors

	17β-Estradiol[a)]	TDP011	TDP012	TDP013	TDP015	TDP044	TDP045	TDP046
# of bound molecules in the H-site	1	1	1	1	2	1[b)]	1	1
GSH requirement for binding	NO	YES	YES	NO	YES	NO	NO	—
GS-conjugation	NO	YES	YES	NO	YES	NO	YES	YES
Interaction with Asp113	YES	NO	NO	NO	NO	YES	YES[c)]	NO
Conformational change of Phe39	NO	YES	YES	YES	YES	NO	NO	NO
Different conformations of the inhibitor in subunits A and B	NO	NO	NO	YES	NO	NO	NO	NO
IC_{50} (μM)	2.33±0.08	6.72±1.48	3.10±0.77	8.94±1.65	3.32±0.81	0.62±0.52	>1000	2.08±0.04

[a)]PDB ID: 6KEP[22] [b)]Electron density map for a whole part of TDP044 was not observed clearly. [c)] TDP045 interacts with Asp113 only when no GSH binds to DmNobo. After conjugation, no interactions with Asp113 were observed.

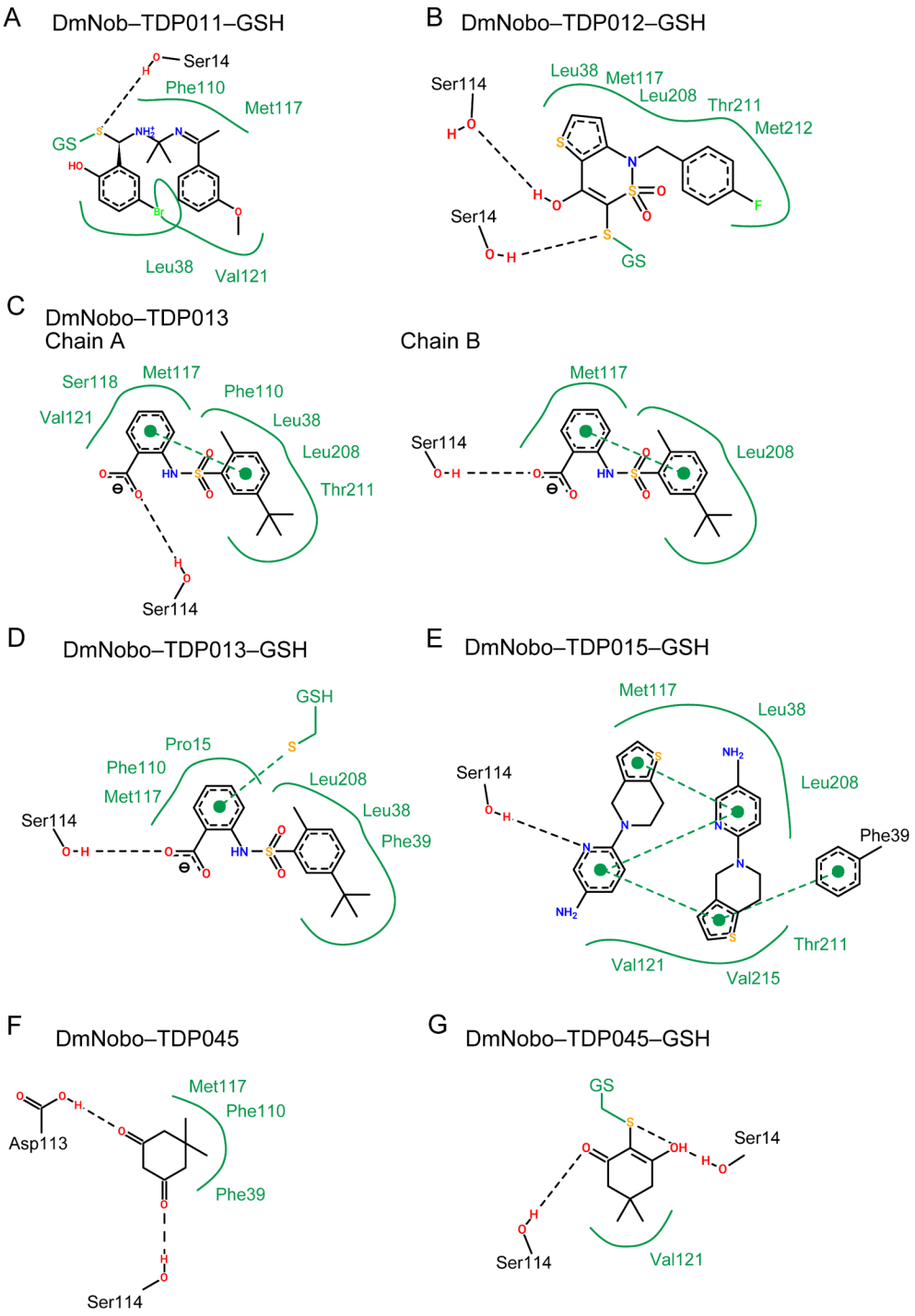

Fig. 3. Illustration of interactions of the identified compounds with DmNobo. (A) DmNobo–TDP011–GSH, (B) DmNobo–TDP012–GSH, (C) DmNobo–TDP013, (D) DmNobo–TDP013–GSH, (E) DmNobo–TDP015–GSH, (F) DmNobo–TDP045, and (G) DmNobo–TDP045–GSH complex structures were drawn using PoseView with manual modifications. Hydrogen bonds are indicated by dotted lines. Hydrophobic interactions and π–π interactions, as predicted by PoseView, are shown as green lines. DmNobo–TDP015 or TDP015–TDP015 interaction was determined by Discovery Studio.

tated at the H-site such that the C2 atom of TDP045 was conjugated with the thiol group of GSH (Fig. 4C and 4D). The covalent bond between TDP045 and GSH was clearly observed in the electron density map (Supplementary Fig. S1G), which was identical to the electron density map of chemically synthesized GS-dimedone (hereafter TDP046) (Supplementary Fig. S1H), indicating that TDP045 in DmNobo crystals is glutathionylated at the C2 atom.

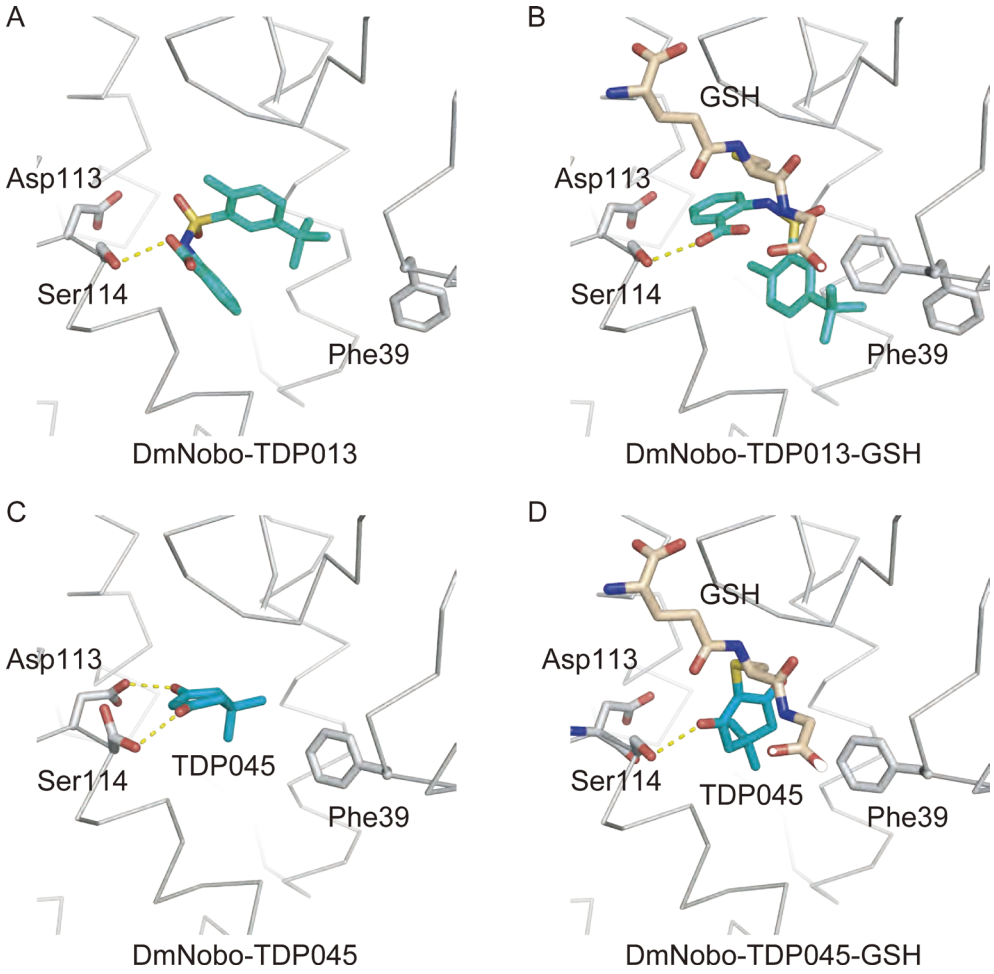

Fig. 4. TDP013 and TDP045 can bind DmNobo with or without GSH. Positions of TDP013 and GSH in the DmNobo pocket are illustrated. (A) TDP013 (carbon in cyan). (B) TDP013 and GSH. (C) TDP045 (carbon in light blue). (D) TDP045 with GSH.

5. GSH-dependent interaction

Under crystallographic conditions in this study, no electron densities of TDP011, TDP012, and TDP015 were observed in the absence of GSH (Supplementary Fig. S2A, B, C). However, electron densities of these inhibitors could be clearly observed in the presence of GSH. In addition, continuous electron densities were observed between these inhibitors and GSH (Supplementary Fig. S1A, B, E). These results suggest that TDP011, TDP012, and TDP015 require GSH for binding with DmNobo at the H-site.

TDP011 structure has three rings (A to C). The electron density map of the DmNobo–TDP011 complex suggested that conjugation with GSH opened the B-ring, resulting in a two-ring structure (Fig. 5A and Supplementary Fig. S3). The TDP011 part of the conjugated structure formed no direct or indirect hydrogen bond interactions with the protein. In the TDP012 complex, the TDP012 part of the conjugated structure formed two hydrogen bonds with Ser14 and Ser114 (Fig. 5C and 5D).

The interaction of TDP015 with DmNobo was rather unique. Two TDP015 molecules bound a single H-site of DmNobo (Fig. 5E). The electron density map suggested that the amino group in the aminopyridine moiety of one TDP015 molecule formed a covalent bond with the Sγ atom of GSH. The conjugated TDP015 molecule showed a kinked conformation, and the other non-conjugated TDP015 molecule showed a stretched conformation. Only one hydrogen bond was formed between the TDP015 molecules and DmNobo (Fig. 3E).

6. Comparisons of compound conformations between subunits

DmNobo is a dimeric protein, and each subunit harbors an H-site for compound binding. There are minor structural and/or physicochemical differences between subunits A and B. GS-TDP011 (hereafter, a compound in the crystal structure conjugated with GSH is indicated by the addition of GS), and GS-TDP013 showed conformational differences between subunits A and B. Simulated annealing-omit maps of the compounds were rather weak (Supplementary Fig. S1). These observations are consistent with the IC_{50} values of these compounds (Fig. 2, Table 1), which were larger than those of the other inhibitors. Structural and/or physicochemical differences between the two H-sites may affect TDP011 and TDP013 conformation.

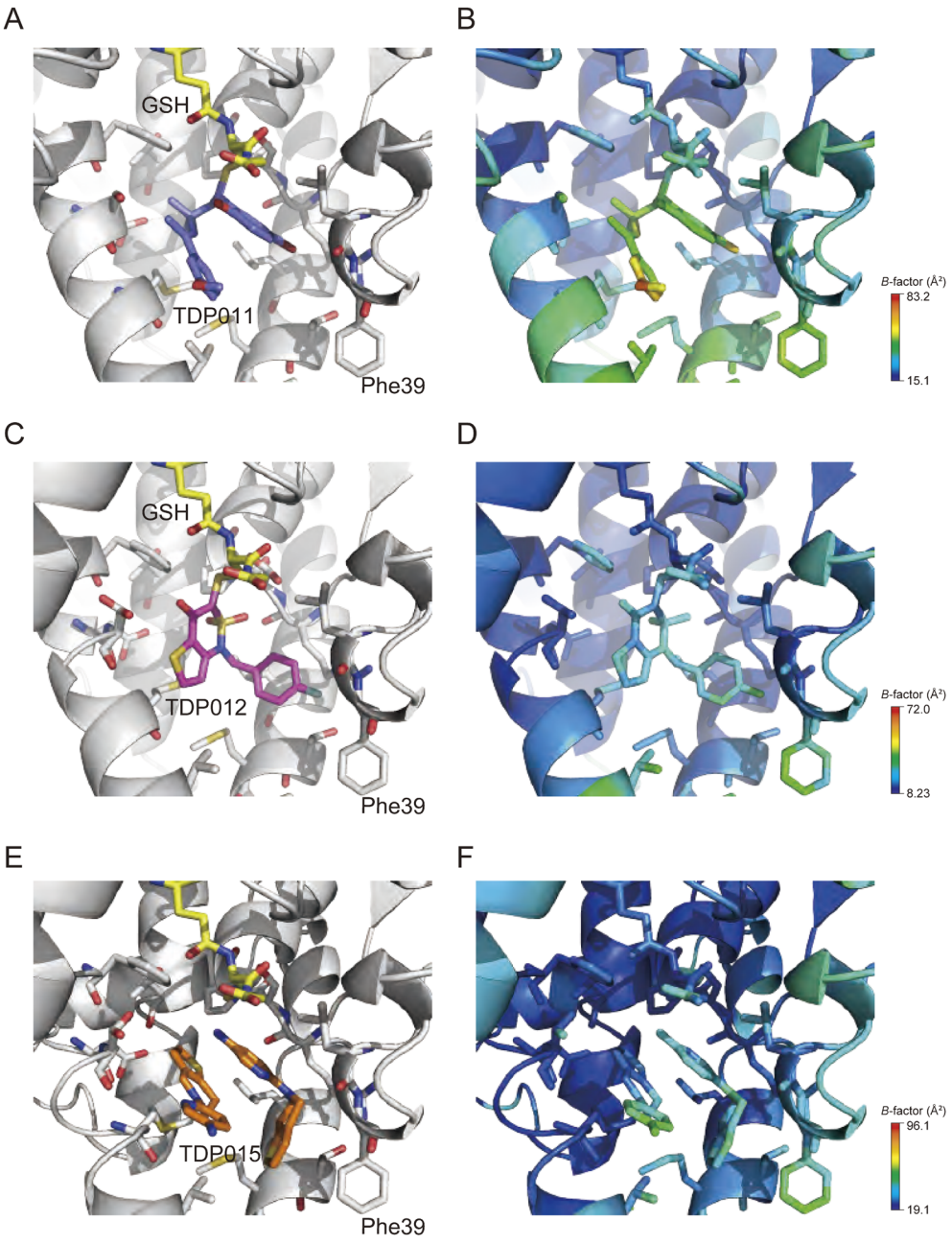

Fig. 5. TDP011, TDP012, and TDP015 can bind DmNobo with GSH. Positions of TDP011, TDP012, TDP015, and GSH in the DmNobo pocket are illustrated. The carbon structure of GSH is shown in yellow in A, C, and E. Rainbow colors in B, D, and F represent temperature factors (*B*-factors, Å^2) of the inhibitor and protein atoms, respectively. (A and B) TDP011 (A, carbon in blue). (C and D) TDP012 (C, carbon in red). (E and F) TDP015 (E, carbon in orange).

7. Structural comparison of EST and the newly identified compounds at the H-site

It has been reported that DmNobo interacts with EST *via* the hydrogen bond with Asp113 and the hydrophobic interactions with other amino acids of H-sites.[22] While the newly identified compounds also formed hydrophobic interactions with DmNobo (Fig. 3), the mode of these hydrophobic interactions differed between EST and the newly identified compounds. Structural comparisons revealed that atoms of the compounds were frequently located in the space that the EST atoms did not occupy. Three small spaces were noted around EST (Fig. 6). First, space A was located below EST, that is between EST and surface A that was composed of Met117, Val121, Thr211, Met212, and Val215. Second, space B was located at the side of EST, that is between EST and surface B that was lined by Arg13, Ser14, Pro15 Leu38, Phe39, and Leu208. Finally, space C was located on the other side of EST, that is between EST surface C that was lined by Phe110, Asp113, Ser114, and Thr169. Atoms of the compounds

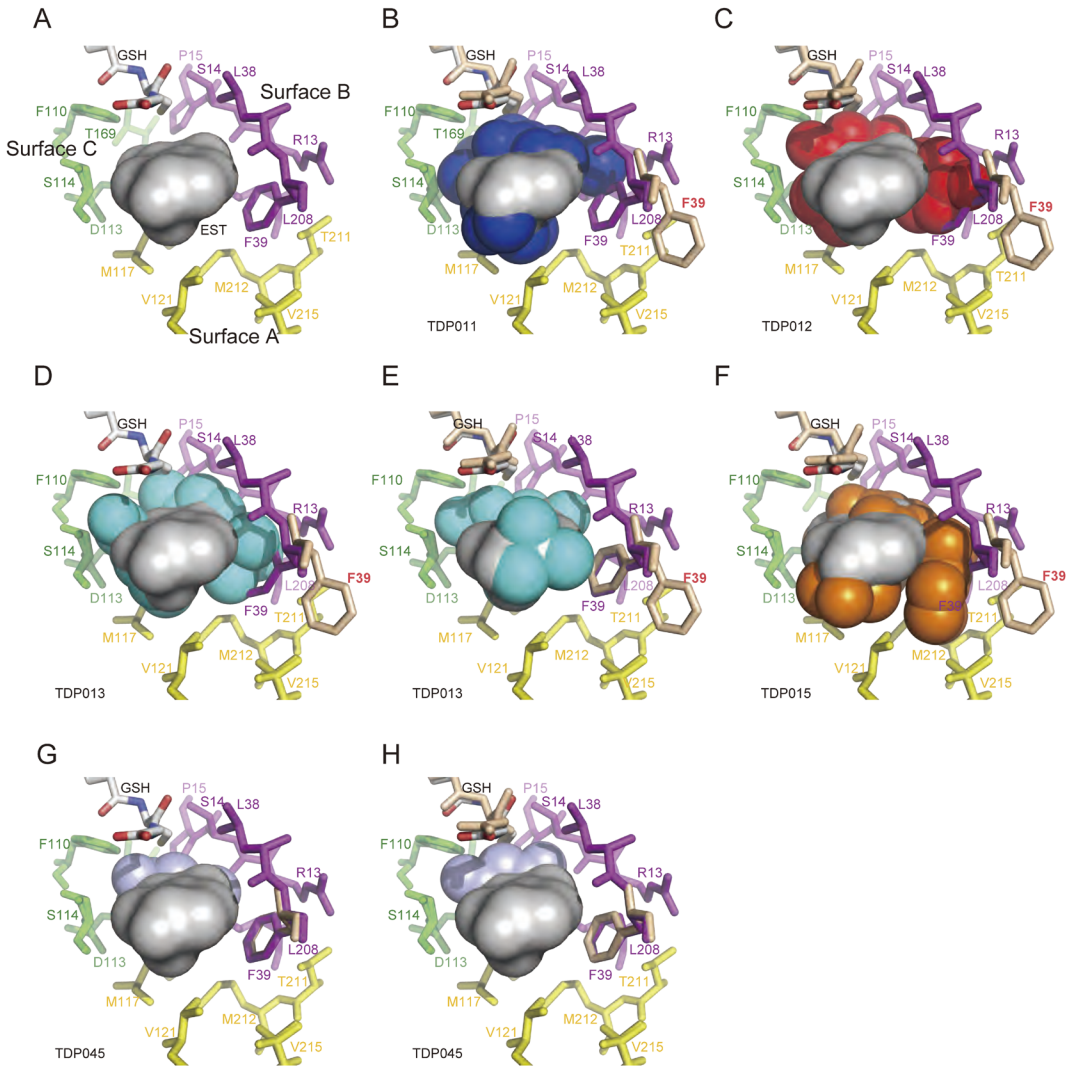

Fig. 6. Interactions of the new compounds with DmNobo. Residue-forming surfaces A, B, and C are shown in yellow, purple, and green, respectively. EST molecules in the surface representation are shown in light gray. Crystal structures of DmNobo in complex with the newly identified compounds are superposed on the crystal structure of the DmNobo–EST complex, and compounds in the DmNobo–EST structure are shown with sphere representation. (A) EST. (B) GS-TDP011 (blue). (C) GS-TDP012 (red). (D) TDP013 (cyan). (E) GS-TDP013. (F) GS-TDP015 (orange). (G) TDP045 (blue light). (H) GS-TDP045. GSH molecules in the EST complex and other complexes are shown in white and peach, respectively. Protruded volumes of the atoms of the new compounds from that of EST are indicated in spaces A, B, and C.

utilized these spaces (or the inner surface of the H-site) (Fig. 6). Since most of the compounds have a non-planar structure, they need to use parts of spaces A, B, and C to be accommodated at the H-site. In some cases, space B was expanded by the conformational change of Phe39 (see below).

8. Conformational changes of residues at H-site

Structural comparison between the apo and compound-bound forms revealed conformational changes of residues at the H-site. DmNobo shows a conformational change of the side chain of Asp113 upon EST binding, forming a hydrogen bond between EST and Asp113.[22] Meanwhile, most of the compounds identified in this study did not form hydrogen bonds with Asp113. Therefore, no conformational changes were observed in Asp113 of DmNobo upon binding with any compound, except TDP045 (Fig. 7A).

As described above, one carbonyl group of TDP045 formed a hydrogen bond with Asp113 (2.6 Å) and the other interacted with Ser114 (2.7 Å). The $\chi 1$ angle of Asp113 was rotated by ~25°, resulting in the formation of a hydrogen bond. In the DmNobo–TDP045–GSH complex, Asp113 did not show a conformational change. GSH conjugation of TDP045 changed its orientation at the H-site, losing the interaction with Asp113.

While the newly identified compounds, except TDP045, induced conformational changes of Asp113, some led to conformational changes of Phe39 (Fig. 7A). The bromophenol group of TDP011, the fluorobenzyl group of TDP012, the *tert*-butyl group of TDP013, and the thienopyridine group of the kinked TDP015

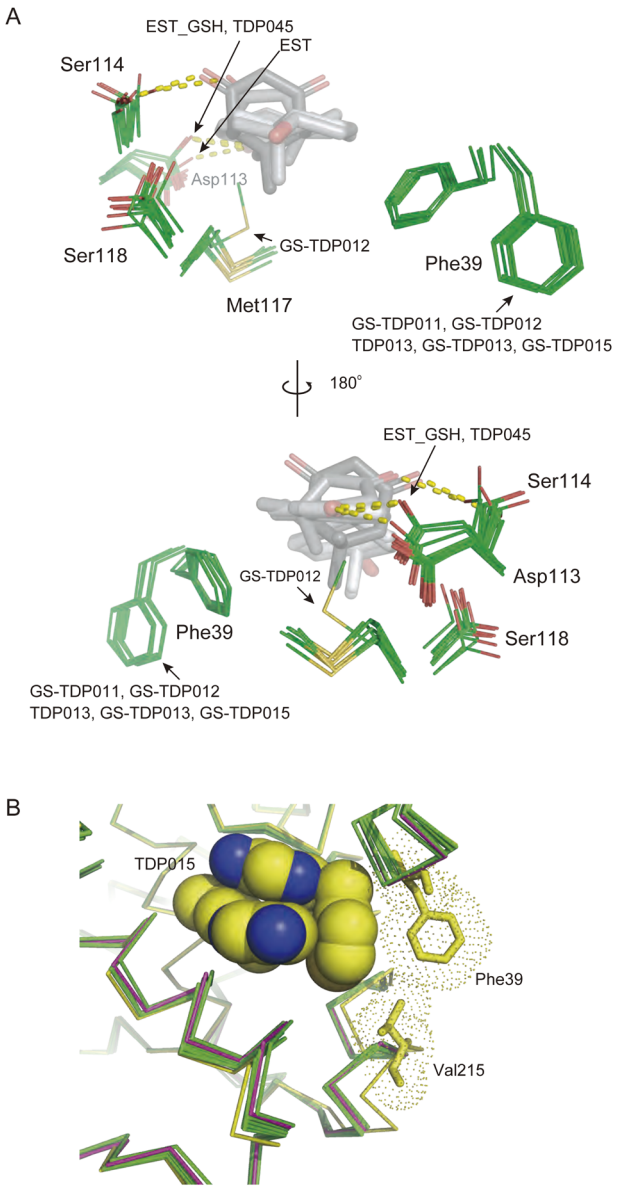

Fig. 7. Conformational changes of residues at the H-site. (A) Conformational changes of Phe39 were most frequently observed in this study. All structures in this study, DmNobo–EST, and the DmNobo–EST–GSH complex were superposed. Hydrogen bonds are shown by dashed lines. (B) Conformational changes around Phe39 observed in the DmNobo–TDP015–GSH complex (yellow). Both DmNobo–EST–GSH complex (purple) and the other structures determined in this study (green) were superposed.

molecule clashed with the side chain of Phe39; therefore, binding of TDP011, TDP012, and TDP015 rotated the side chain of Phe39, exposing Thr211 and Val215 on the inner surface of H-site. The thienopyridine group of the kinked TDP015 molecule interacted with Val215, and the main chain atoms around Val215 showed significant shifts from their original position (Fig. 7B).

9. Phe39 flexibility calculated by MD simulation

Structural analysis showed that the inhibitors TDP011, TDP012, TDP013, and TDP015 induced a conformational change of Phe39 from a closed to an open form. However, the crystal structure of the DmNobo–EST–GSH complex did not show a conformational change of Phe39.[21,22] Our previous MD simulations of the DmNobo–EST–GSH complex suggested that Phe39 is stable and remained in a closed form.[22] Here, we performed MD simulations for DmNobo in apo and GSH-complexed forms (Fig. 8) and demonstrated that Asp113 was stable at the EST-bound form during simulation; however, the open form of Phe39 was often simulated (Fig. 8C and 8D). These results suggest that Phe39 is mobile without EST and can easily undergo a conformational change.

Discussion

In this study, we identified five small non-steroidal compounds that inhibit the GSH-conjugating activity of DmNobo. The crystal structures of DmNobo complexed with these inhibitors and their derivative suggested that the H-site of DmNobo harbors hydrophobic targets for compounds other than the previously identified ones using EST. These compounds and their complex structures with DmNobo will be beneficial for developing novel IGRs targeting Nobo and new drugs against other GSTs.

Our previous study showed that Asp113 is essential for the binding of DmNobo with EST,[22] indicating that this residue can serve as a target for IGR development. Among the five compounds identified in this study, only one compound—TDP045—interacted with Asp113 for binding. Notably, however, the carbon skeletons with functional groups, which are required for interaction with DmNobo, largely differ between EST and TDP045. EST contains an aromatic ring with a hydroxyl group, while TDP045 contains a non-aromatic ring with carbonyl and/or hydroxyl groups. Since these functional groups of TDP045 form a hydrogen bond with Asp113, DmNobo is unlikely to require an aromatic ring for forming a complex through this residue. Considering that Asp113 of DmNobo is essential for ecdysteroid biosynthesis,[22] an unknown endogenous substrate of DmNobo containing non-aromatic A-rings likely serves as an intermediate in ecdysteroid biosynthesis. Notably, a recent study reported that DmNobo shows isomerase activity against Δ5-androstene-3,17-dione, in which a ketone group is located on a cyclohexane group in the A-ring.[21]

Crystal structures of DmNobo with the identified inhibitors suggested that hydrophobic residues, particularly Leu38, Phe39, Leu208, and Met117, at the H-site mainly contribute to the binding of these inhibitors (Fig. 3). Among these hydrophobic residues, Phe39 is unique. It undergoes a conformational change upon inhibitor binding (TDP011, TDP012, and TDP015), such that Thr211 and Val215 on the inner surface of the H-site are exposed. A buried hydrophobic surface composed of Thr211 and Val215 can, therefore, serves as a target for DmNobo inhibitors. Despite the observed conformational changes of Phe39, we do not think that similar conformational changes occur *in vivo* to bind an unidentified substrate of Nobo. Since Phe39 is highly conserved among Nobo proteins,[22] it is reasonable to consider

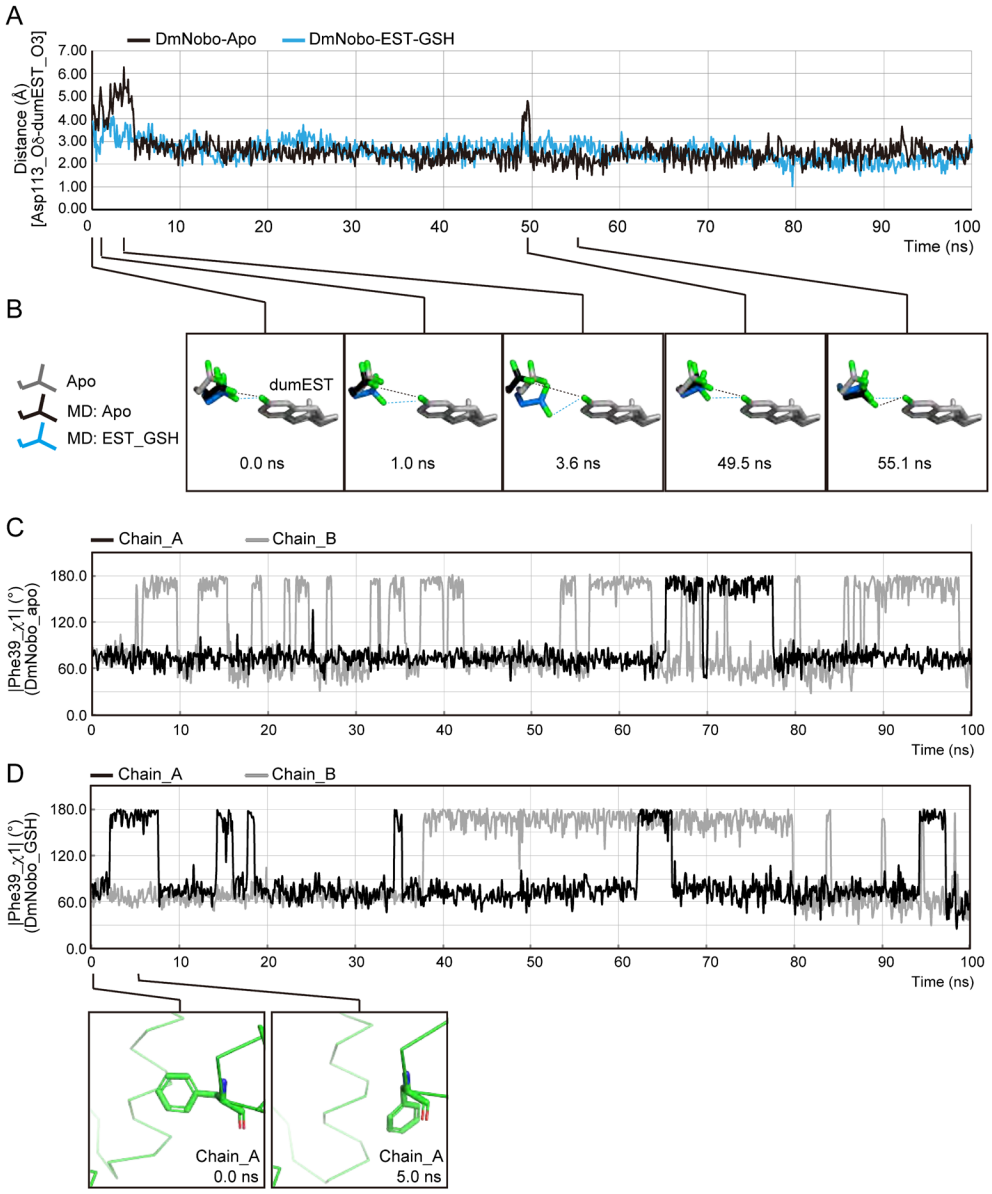

Fig. 8. Molecular dynamics simulations of DmNobo in apo and GSH complex forms. Molecular dynamics simulation of DmNobo–Apo and DmNobo–GSH was performed for 100 nsec at 300 K with water molecules. (A) Distance between the Oδ atom of Asp113 and the O3 atom of a dummy EST molecule. The dummy EST molecule (dumEST) was placed in the models at 0 nsec by superposition of Cα atoms of chain A of DmNobo–EST–GSH. The coordinate of the O3 atom of the dumEST was extracted, and the distance between the Oδ atom of Asp113 at each frame and the O3 atom of the dumEST was calculated. The distances in DmNobo–Apo (black) and DmNobo–EST–GSH (blue) were plotted. (B) Snapshots of Asp113 at the indicated frames. The Cα atoms of chain A of the crystal structure of DmNobo–Apo (gray) were superimposed with those of an MD model of DmNobo–Apo (MD: Apo) at 0 nsec. Cα atoms of chain A of DmNobo–EST–GSH (MD: EST–GSH) were superposed with those of DmNobo–Apo. The absolute values of the χ1 torsion angle of Phe39 of chains A (black line) and B (gray line) of DmNobo–Apo (C) and DmNobo–GSH (D) were plotted. Representative MD models of DmNobo–GSH with open- and closed-form Phe39 are shown, whose absolute values of χ1 torsion angle are ∼75° at 0.0 nsec and ∼175° at 5.0 nsec.

that the substrate of Nobo interacts with Phe39 in the closed form. Conversely, Thr211 and Val215 are not conserved, suggesting that the unidentified substrate is unlikely to interact with Thr211 and Val215.

TDP015 has a unique binding mode. Two TDP015 molecules bind at the H-site. Of these two, the kinked TDP015 molecule interacts with the exposed Thr211 and Val215 as well as with Phe39, while the other TDP015 molecule forms hydrophobic interactions with residues lining the H-site and π–π interactions with the kinked molecule. Despite these interactions, however, the IC_{50} value of TDP015 was comparable to that of the other compounds. This may be due to entropy loss caused by the binding of two molecules and lack of interaction with Asp113. Considering the higher temperature factors for the inhibitor atoms (Fig. 5), hydrophobic interactions may not be sufficient for stable binding of these inhibitors. Conformational differences be-

tween subunits A and B of TDP013, GS-TDP013, and TDP011 (Fig. 4) also support this notion. These weak interactions could be compensated by conjugation with GSH. To improve the affinity of TDP015 to DmNobo, (1) a linkage between the two TDP015 molecules may be required to avoid entropy loss and (2) a hydrophilic group may be added to facilitate interaction with Asp113.

In this study, we found that compounds, TDP011, TDP012, TDP015, and TDP045 were glutathionylated in the presence of GSH. The glutathionylation should not be enzymatically reacted because it needs sulfenylation of the Sγ atom, and may be due to oxidation during crystal preparation. However, these structures can be informative for further development of inhibitors with higher activity. Indeed, from the crystal structure of DmNobo–TDP045–GSH, we could design a novel inhibitor against the G-site of DmNobo, GS-dimedone (TDP046 in this study). By application of the conjugated products, we expect that we can also develop novel inhibitors with higher specificity and inhibitory activity.

In conclusion, we identified five novel Nobo inhibitors, which might be useful for developing new IGRs targeting ecdysteroid biosynthesis. These inhibitors interact with the H-site of DmNobo mainly through hydrophobic interactions. Structural analysis revealed strategies to increase their affinities to DmNobo.

Acknowledgements

We thank Dr. Yusuke Yamada for managing the automated data collection at the Photon Factory; Dr. Mikio Tanabe for managing a beamtime at the Taiwan Photon Source; and Dr. Tetsuo Nagano for continuous encouragement and kind advice. We would also like to thank Editage (www.editage.com) for English language editing. This work was supported in part by a KEK Postgraduate Research Student fellowship to K.I. This work was also supported by KAKENHI (grant numbers 15K14719 and 18K19163) to R.N. and by the Private University Research Branding Project to Y.F. In addition, this research was partially supported by the Platform Project for Supporting Drug Discovery and Life Science Research from AMED under grant number JP19am0101086 (support number 1290). This work was performed with the approval of the Photon Factory Program Advisory Committee (proposal number 2018G025).

Electronic supplementary materials

The online version of this article contains supplementary materials (Supplemental Schemes S1–S3, Figs. S1–S3, Tables S1, S2), which are available at http://www.jstage.jst.go.jp/browse/jpestics/.

References

1) C. M. Williams: Third-generation pesticides. *Sci. Am.* **217**, 13–17 (1967).
2) X. Pan, R. P. Connacher and M. B. O'Connor: Control of the insect metamorphic transition by ecdysteroid production and secretion. *Curr. Opin. Insect Sci.* **43**, 11–20 (2020).
3) R. Niwa and Y. S. Niwa: Enzymes for ecdysteroid biosynthesis: their biological functions in insects and beyond. *Biosci. Biotechnol. Biochem.* **78**, 1283–1292 (2014).
4) L. I. Gilbert: Halloween genes encode P450 enzymes that mediate steroid hormone biosynthesis in *Drosophila melanogaster*. *Mol. Cell. Endocrinol.* **215**, 1–10 (2004).
5) H. Chanut-Delalande, Y. Hashimoto, A. Pelissier-Monier, R. Spokony, A. Dib, T. Kondo, J. Bohère, K. Niimi, Y. Latapie, S. Inagaki, L. Dubois, P. Valenti, C. Polesello, S. Kobayashi, B. Moussian, K. P. White, S. Plaza, Y. Kageyama and F. Payre: Pri peptides are mediators of ecdysone for the temporal control of development. *Nat. Cell Biol.* **16**, 1035–1044 (2014).
6) S. Enya, T. Ameku, F. Igarashi, M. Iga, H. Kataoka, T. Shinoda and R. Niwa: A Halloween gene *noppera-bo* encodes a glutathione *S*-transferase essential for ecdysteroid biosynthesis *via* regulating the behaviour of cholesterol in *Drosophila*. *Sci. Rep.* **4**, 6586 (2014).
7) S. Enya, T. Daimon, F. Igarashi, H. Kataoka, M. Uchibori, H. Sezutsu, T. Shinoda and R. Niwa: The silkworm glutathione S-transferase gene noppera-bo is required for ecdysteroid biosynthesis and larval development. *Insect Biochem. Mol. Biol.* **61**, 1–7 (2015).
8) T. Yoshiyama, T. Namiki, K. Mita, H. Kataoka and R. Niwa: Neverland is an evolutionally conserved Rieske-domain protein that is essential for ecdysone synthesis and insect growth. *Development* **133**, 2565–2574 (2006).
9) T. Yoshiyama-Yanagawa, S. Enya, Y. Shimada-Niwa, S. Yaguchi, Y. Haramoto, T. Matsuya, K. Shiomi, Y. Sasakura, S. Takahashi, M. Asashima, H. Kataoka and R. Niwa: The conserved rieske oxygenase DAF-36/Neverland is a novel cholesterol-metabolizing enzyme. *J. Biol. Chem.* **286**, 25756–25762 (2011).
10) R. Niwa, T. Namiki, K. Ito, Y. Shimada-Niwa, M. Kiuchi, S. Kawaoka, T. Kayukawa, Y. Banno, Y. Fujimoto, S. Shigenobu, S. Kobayashi, T. Shimada, S. Katsuma and T. Shinoda: *Non-molting glossy/shroud* encodes a short-chain dehydrogenase/reductase that functions in the 'Black Box' of the ecdysteroid biosynthesis pathway. *Development* **137**, 1991–1999 (2010).
11) T. Namiki, R. Niwa, T. Sakudoh, K. I. Shirai, H. Takeuchi and H. Kataoka: Cytochrome P450 CYP307A1/Spook: A regulator for ecdysone synthesis in insects. *Biochem. Biophys. Res. Commun.* **337**, 367–374 (2005).
12) H. Ono, K. F. Rewitz, T. Shinoda, K. Itoyama, A. Petryk, R. Rybczynski, M. Jarcho, J. T. Warren, G. Marqués, M. J. Shimell, L. I. Gilbert and M. B. O'Connor: *Spook* and *Spookier* code for stage-specific components of the ecdysone biosynthetic pathway in Diptera. *Dev. Biol.* **298**, 555–570 (2006).
13) Q. Ou, A. Magico and K. King-Jones: Nuclear receptor DHR4 controls the timing of steroid hormone pulses during *Drosophila* development. *PLoS Biol.* **9**, e1001160 (2011).
14) R. Niwa, T. Matsuda, T. Yoshiyama, T. Namiki, K. Mita, Y. Fujimoto and H. Kataoka: CYP306A1, a cytochrome P450 enzyme, is essential for ecdysteroid biosynthesis in the prothoracic glands of *Bombyx* and *Drosophila*. *J. Biol. Chem.* **279**, 35942–35949 (2004).
15) J. T. Warren, A. Petryk, G. Marqués, J. P. Parvy, T. Shinoda, K. Itoyama, J. Kobayashi, M. Jarcho, Y. Li, M. B. O'Connor, C. Dauphin-Villemant and L. I. Gilbert: Phantom encodes the 25-hydroxylase of *Drosophila melanogaster* and *Bombyx mori*: A P450 enzyme critical in ecdysone biosynthesis. *Insect Biochem. Mol. Biol.* **34**, 991–1010 (2004).
16) J. T. Warren, A. Petryk, G. Marques, M. Jarcho, J.-P. Parvy, C. Dauphin-Villemant, M. B. O'Connor and L. I. Gilbert: Molecular and biochemical characterization of two P450 enzymes in the ecdysteroidogenic pathway of *Drosophila melanogaster*. *Proc. Natl. Acad. Sci. U.S.A.* **99**, 11043–11048 (2002).
17) A. Petryk, J. T. Warren, G. Marques, M. P. Jarcho, L. I. Gilbert, J. Kahler, J.-P. Parvy, Y. Li, C. Dauphin-Villemant and M. B. O'Connor: Shade is the *Drosophila* P450 enzyme that mediates the hydroxylation

of ecdysone to the steroid insect molting hormone 20-hydroxyecdysone. *Proc. Natl. Acad. Sci. U.S.A.* **100**, 13773–13778 (2003).
18) V. M. Chávez, G. Marques, J. P. Delbecque, K. Kobayashi, M. Hollingsworth, J. Burr, J. E. Natzle and M. B. O'Connor: The *Drosophila disembodied* gene controls late embryonic morphogenesis and codes for a cytochrome P450 enzyme that regulates embryonic ecdysone levels. *Development* **127**, 4115–4126 (2000).
19) J. Saito, R. Kimura, Y. Kaieda, R. Nishida and H. Ono: Characterization of candidate intermediates in the Black Box of the ecdysone biosynthetic pathway in *Drosophila melanogaster*: Evaluation of molting activities on ecdysteroid-defective larvae. *J. Insect Physiol.* **93–94**, 94–104 (2016).
20) C. Saisawang, J. Wongsantichon and A. J. Ketterman: A preliminary characterization of the cytosolic glutathione transferase proteome from *Drosophila melanogaster*. *Biochem. J.* **442**, 181–190 (2012).
21) J. Škerlová, H. Lindström, E. Gonis, B. Sjödin, F. Neiers, P. Stenmark and B. Mannervik: Structure and steroid isomerase activity of *Drosophila* glutathione transferase E14 essential for ecdysteroid biosynthesis. *FEBS Lett.* **594**, 1187–1195 (2020).
22) K. Koiwai, K. Inaba, K. Morohashi, S. Enya, R. Arai, H. Kojima, T. Okabe, Y. Fujikawa, H. Inoue, R. Yoshino, T. Hirokawa, K. Kato, K. Fukuzawa, Y. Shimada-Niwa, A. Nakamura, F. Yumoto, T. Senda and R. Niwa: An integrated approach to unravel a crucial structural property required for the function of the insect steroidogenic Halloween protein Noppera-bo. *J. Biol. Chem.* **295**, 7154–7167 (2020).
23) B. Wu and D. Dong: Human cytosolic glutathione transferases: Structure, function, and drug discovery. *Trends Pharmacol. Sci.* **33**, 656–668 (2012).
24) S. Enya, C. Yamamoto, H. Mizuno, T. Esaki, H.-K. Lin, M. Iga, K. Morohashi, Y. Hirano, H. Kataoka, T. Masujima, Y. Shimada-Niwa and R. Niwa: Dual Roles of glutathione in ecdysone biosynthesis and antioxidant function during the larval development in *Drosophila*. *Genetics* **207**, 1519–1532 (2017).
25) Y. Fujikawa, F. Morisaki, A. Ogura, K. Morohashi, S. Enya, R. Niwa, S. Goto, H. Kojima, T. Okabe, T. Nagano and H. Inoue: A practical fluorogenic substrate for high-throughput screening of glutathione *S*-transferase inhibitors. *Chem. Commun. (Camb.)* **51**, 11459–11462 (2015).
26) W. Kabsch: Xds. *Acta Crystallogr. D Biol. Crystallogr.* **66**, 125–132 (2010).
27) P. Evans: Scaling and assessment of data quality. *Acta Crystallogr. D Biol. Crystallogr.* **62**, 72–82 (2006).
28) P. R. Evans and G. N. Murshudov: How good are my data and what is the resolution? *Acta Crystallogr. D Biol. Crystallogr.* **69**, 1204–1214 (2013).
29) Y. Yamada, N. Matsugaki, L. M. G. Chavas, M. Hiraki, N. Igarashi and S. Wakatsuki: Data management system at the photon factory macromolecular crystallography beamline. *J. Phys. Conf. Ser.* **425**, 1–4 (2013).
30) A. Vagin and A. Teplyakov: MOLREP : an Automated program for molecular replacement. *J. Appl. Cryst.* **30**, 1022–1025 (1997).
31) G. N. Murshudov, A. A. Vagin and E. J. Dodson: Refinement of macromolecular structures by the maximum-likelihood method. *Acta Crystallogr. D Biol. Crystallogr.* **53**, 240–255 (1997).
32) P. Emsley, B. Lohkamp, W. G. Scott and K. Cowtan: Features and development of Coot. *Acta Crystallogr. D Biol. Crystallogr.* **66**, 486–501 (2010).
33) P. V. Afonine, R. W. Grosse-Kunstleve, N. Echols, J. J. Headd, N. W. Moriarty, M. Mustyakimov, T. C. Terwilliger, A. Urzhumtsev, P. H. Zwart and P. D. Adams: Towards automated crystallographic structure refinement with phenix.refine. *Acta Crystallogr. D Biol. Crystallogr.* **68**, 352–367 (2012).
34) K. Stierand and M. Rarey: From modeling to medicinal chemistry: Automatic generation of two-dimensional complex diagrams. *ChemMedChem* **2**, 853–856 (2007).
35) N. R. Voss and M. Gerstein: 3V: Cavity, channel and cleft volume calculator and extractor. *Nucleic Acids Res.* **38**(Web Server), 555–562 (2010).
36) E. Krissinel: Enhanced fold recognition using efficient short fragment clustering. *J. Mol. Biochem.* **1**, 76–85 (2012).
37) J. C. Shelly, A. Cholleti, L. L. Frye, J. R. Greenwood, M. R. Timlin and M. Uchiyama: Epik: A software program for pK(a) prediction and protonation state generation for drug-like molecules. *J. Comput. Aided Mol. Des.* **21**, 681–691 (2007).
38) H. Li, A. D. Robertson and J. H. Jensen: Very fast empirical prediction and rationalization of protein pKa values. *Proteins* **61**, 704–721 (2005).
39) E. Harder, W. Damm, J. Maple, C. Wu, M. Reboul, J. Y. Xiang, L. Wang, D. Lupyan, M. K. Dahlgren, J. L. Knight, J. W. Kaus, D. S. Cerutti, G. Krilov, W. L. Jorgensen, R. Abel and R. A. Friesner: OPLS3: A force field providing broad coverage of drug-like small molecules and proteins. *J. Chem. Theory Comput.* **12**, 281–296 (2016).
40) W. L. Jorgensen, J. Chandrasekhar, J. D. Madura, R. W. Impey and M. L. Klein: Comparison of simple potential functions for simulating liquid water. *J. Chem. Phys.* **79**, 926–935 (1983).